Longitudinal Instability Studies at the SURF II Storage Ring at NIST

K. C. Harkay and N. S. Sereno

Advanced Photon Source, Argonne National Laboratory

July 27, 1998

Abstract

Measurements of the longitudinal instability observed in the storage ring at the Synchrotron Ultraviolet Radiation Facility (SURF II) at the National Institute of Standards and Technology (NIST) were performed to understand the mechanism driving the instability. The instability, studied in depth by Rakowsky and others [1][2], manifests itself in broad resonance features in the horizontal and vertical motion spectrum of the synchrotron light from DC to a few kHz [3]. Also observed are multiple synchrotron harmonics that modulate the revolution harmonics; these are characteristic of longitudinal phase oscillations. These spectral features of the motion are found to be correlated with the periodic lengthening and shortening of the bunch length on time scales from ~0.1 ms to 20 ms, depending on machine and radio-frequency (rf) system parameters. In this report, the growth rate of the instability is determined from measurements using an rf pickup electrode. The measured growth rates are compared to computed growth rates from an analytical model. Recommendations are made regarding options to control or mitigate the instability. In light of upgrade plans for SURF III, a few comments are presented about the beam lifetime.

1.0 Introduction

Beam instabilities are intensity-dependent collective effects that arise as a result of the electromagnetic wake fields generated by the beam as it interacts with its environment. Coherent oscillations appear above some threshold current when the induced wake field forces overwhelm the natural synchrotron radiation damping of the electron beam [4]. The oscillation amplitude grows exponentially in time until either the beam is lost or nonlinearities in the system limit the growth. Such nonlinear fluctuations are extremely difficult to characterize; instead, the approach is to establish the instability risetime while the motion is in the linear regime. The instability risetime is one of the basic input design parameters for an active feedback system used to control the instability. Finally, if one can determine which subsystem or structure in the vacuum chamber is likely to be the driving source of the instability, passive damping techniques may be implemented to reduce the size of the wake fields. It is common to refer to the machine coupling impedance, which is the frequency-domain equivalent of the wake field.

2.0 SURF II Storage Ring Operational Setup

The measurements were carried out on the SURF II weak-focusing storage ring on the last two days of the August 1997 run using standard operating parameters. The nominal machine parameters are listed in Table 1. Time constraints permitted varying only a limited number of operating conditions in order to induce and observe the instability. The machine was typically filled to < 150 mA in two equally filled bunches and ramped to an energy of 256 MeV, at which time the bunch length is about 1 ns (fwhm).

TABLE 1. Nominal SURF-II Storage Ring Parameters

Energy	E	256	MeV
Circumference	C	5.267	m
Bending field, max.	B	1.2	T
Field index	n	0.59	
Harmonic number	h	2	
Rf frequency	f_{rf}	113.8	MHz
Synchrotron frequency	f_s	330	kHz
Rf gap voltage	V_{rf}	10	kV
Synchrotron rad. energy loss/turn	U	0.456	keV
Damping time, longitudinal	τ_z	12.8	ms
Damping time, transverse	$\tau_{x,y}$	13.9	ms
Bunch length, fwhm	τ_L	1	ns
Horizontal, vertical tune	ν_x, ν_y	0.640, 0.768	
Dispersion	D	2.044	m
Momentum compaction	α	2.44	

Assuming that the instability in SURF II is caused by the interaction of the beam with an electromagnetic wake field, we expect to observe the instability at a threshold current that depends on various machine parameters. Beam-excited higher-order modes (HOMs) in the rf cavities are a common source of coupling impedance; therefore, the present studies focused on measuring the risetime of the instability as a function of beam current and rf system parameters. If the oscillation amplitude of the collective motion does saturate due to nonlinearities [5], it is possible that this could result in noise fluctuations of the kind seen at low frequencies and/or the microwave signals seen at high frequencies [6]. This view is supported qualitatively by the correlation between the time dependence of the synchotron oscillations and the low-frequency fluctuations observed during this machine study period. Discussion of the microwave emissions is beyond the scope of this paper.

3.0 Beam Monitoring Diagnostic

Figure 1 shows the time evolution for the instability as observed on a capacitive pickup beam monitor electrode (BME) located in the SURF II storage ring vacuum chamber. The “Q probe,” as it is otherwise known, is a 2-inch-long section of rectangular S-band waveguide. The waveforms in Fig. 1 were acquired using a Hewlett Packard (HP) 54542A 2 Gs/s sampling scope. The two plots show the amplitude variation in the BME signal for two different values of the beam current and rf phase; more will be said about this later. For a Gaussian bunch, the voltage induced on the BME is given by [7],

$$V(t) = \frac{eNZ_{eff}}{\sqrt{2\pi}\sigma(t)}\left\{\exp\left(\frac{-(t+\tau)^2}{2\sigma(t)^2}\right) - \exp\left(\frac{-(t-\tau)^2}{2\sigma(t)^2}\right)\right\} \tag{1}$$

where $\sigma(t)$ is the rms bunch length, which typically varies with time when the beam is unstable, eN is the charge in the bunch and Z_{eff} is the effective BME transmission line impedance. The above signal shape repeats in SURF II at twice the revolution period of $1/f_{rf}$ (harmonic number of 2). There are two time scales of interest in Eq. (1). The first is a fast time scale defined by the parameter τ, which represents the time it takes a signal to propagate the length of the electrode (~ 0.17 ns for the SURF II BME). The second time scale is implicitly defined by the variation of the bunch length parameter, $\sigma(t)$. In Fig. 1, the amplitude variation of the BME signals is a result of the rms bunch length change due to the instability. This motion is observed to vary with a broad period of between 15 and 19 ms depending on machine parameters.

Maximum amplitude in the figure corresponds to a minimum bunch length. When the instability occurs, the bunch length varies on a time scale that is long compared to time scales defined by the bunch length and revolution time, but is comparable to the radiation damping time of 13 ms, given in Table 1. When the beam intensity is high, there is additional structure within the broad periodicity (Fig. 1b), and there is an associated variation in the growth rates of the synchrotron sideband power, discussed in the next section.

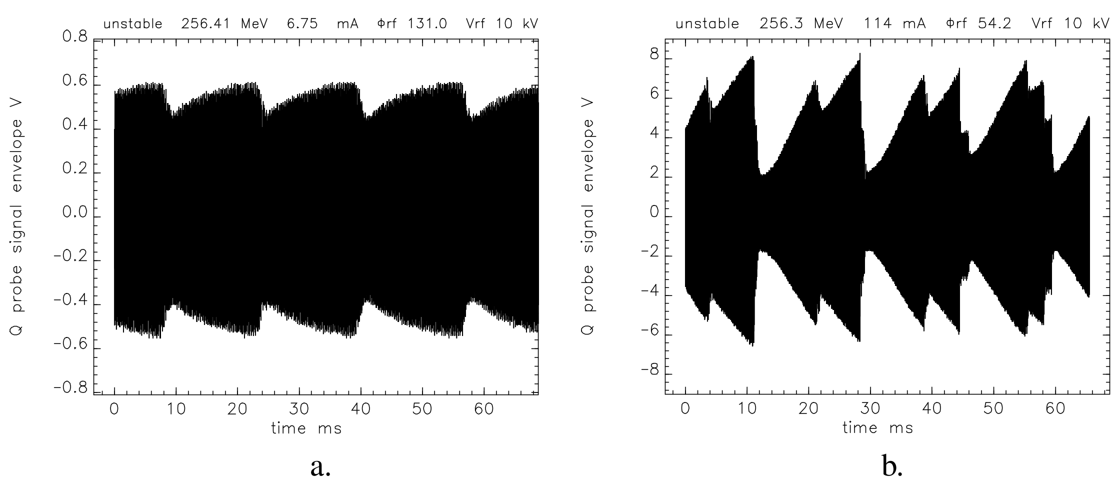

FIGURE 1. Time domain BME signal when the instability is active at two different stored currents: (a) 6.9 mA and (b) 114 mA. The vertical scales are not the same.

Qualitatively, the low-frequency horizontal and vertical spectra taken by observing the synchrotron light can be described in terms of the instability [3]. As the bunch length and hence energy spread fluctuates under the influence of the instability, the horizontal beam size is modulated due to the large dispersion (~2 m). For the case of the vertical plane, residual dispersion and/or coupling in the machine result in the observed motion.

4.0 Instability Growth Rate and Frequency Shift Measurements

The instability threshold was found to be very sensitive to the phase between the radio-frequency (rf) generator and the rf accelerating cavity. A phase shifter allows this phase to be changed. The phase shifter was installed after the papers of Refs. [1][2]. At specific values of the phase, the instability could be excited with as little as 7 mA of beam, albeit less severely than at higher currents (Fig. 1.) A likely explanation for this is that the beam-excited HOMs couple out of the cavity into the rf drive transmission line. Because the line is matched only at the fundamental rf frequency, the HOMs can be reflected back into the cavity and, depending on the rf phase, the HOM fields may add constructively at the gap and be large enough to drive the beam. Rf bench measurements of the cavity-transmission line system were performed and show a large contribution at the gap of the HOM at approximately 342 MHz; these results are discussed in Section 5. Another observation is that the beam could be stabilized by reducing the rf voltage from 10 kV to 8 kV, which increases the nonlinearity of motions of a given amplitude inside the rf bucket (qualitatively observed in [1].)

The instability signature was measured in the frequency domain by recording the BME signal using an HP 89441A Vector Signal Analyzer (VSA). The capture buffer feature of the VSA provides a signal spectrum as a function of time by acquiring a long sample and then performing a fast Fourier transform on a series of subsamples of a given length. The instability manifests itself as amplitude growth and a frequency shift of certain synchrotron sidebands around primarily the even revolution harmonics. A total of seven sets of data were acquired for various settings of the rf phase angle and beam current while keeping the beam energy and rf voltage constant. The machine conditions for these datasets are listed in Table 2. The phase shifter position is uncalibrated. The beam energy was 256.3 MeV for machine conditions 1-4 and 256.6 MeV for conditions 5-7. Time domain waveforms were also acquired using the HP 54542A sampling scope.

TABLE 2. SURF II Machine Conditions for Captured Spectral Datasets

Machine condition	beam current (mA)	rf voltage (kV)	rf phase shifter (deg)	center freq (MHz)	rev harm (2 x rf harm)	stable or unstable?
1	113	10	54.2	113.846	2	U
2	~100	10	54.2	113.846	2	U
3	~94	10	54.2	569.230	10	U
4	88	10	68.8	569.230	10	S
5	83	9.7	89.6	341.538	6	U
6	78	9.8	89.6	398.461	7	U
7	76	9.8	89.6	626.153	11	U

Figure 2 shows typical spectra at the third rf harmonic (341.5 MHz) observed when the instability cycles through maximum amplitude. As many as five synchrotron harmonics can be seen. The horizontal scale is frequency relative to the third rf harmonic and the snapshot times are relative to the start of data acquisition. The machine parameters for these data were 83 mA, 9.7 kV rf voltage, and 89.6 degrees rf phase (machine condition 5). A synchrotron frequency of 330 kHz is obtained from these data.

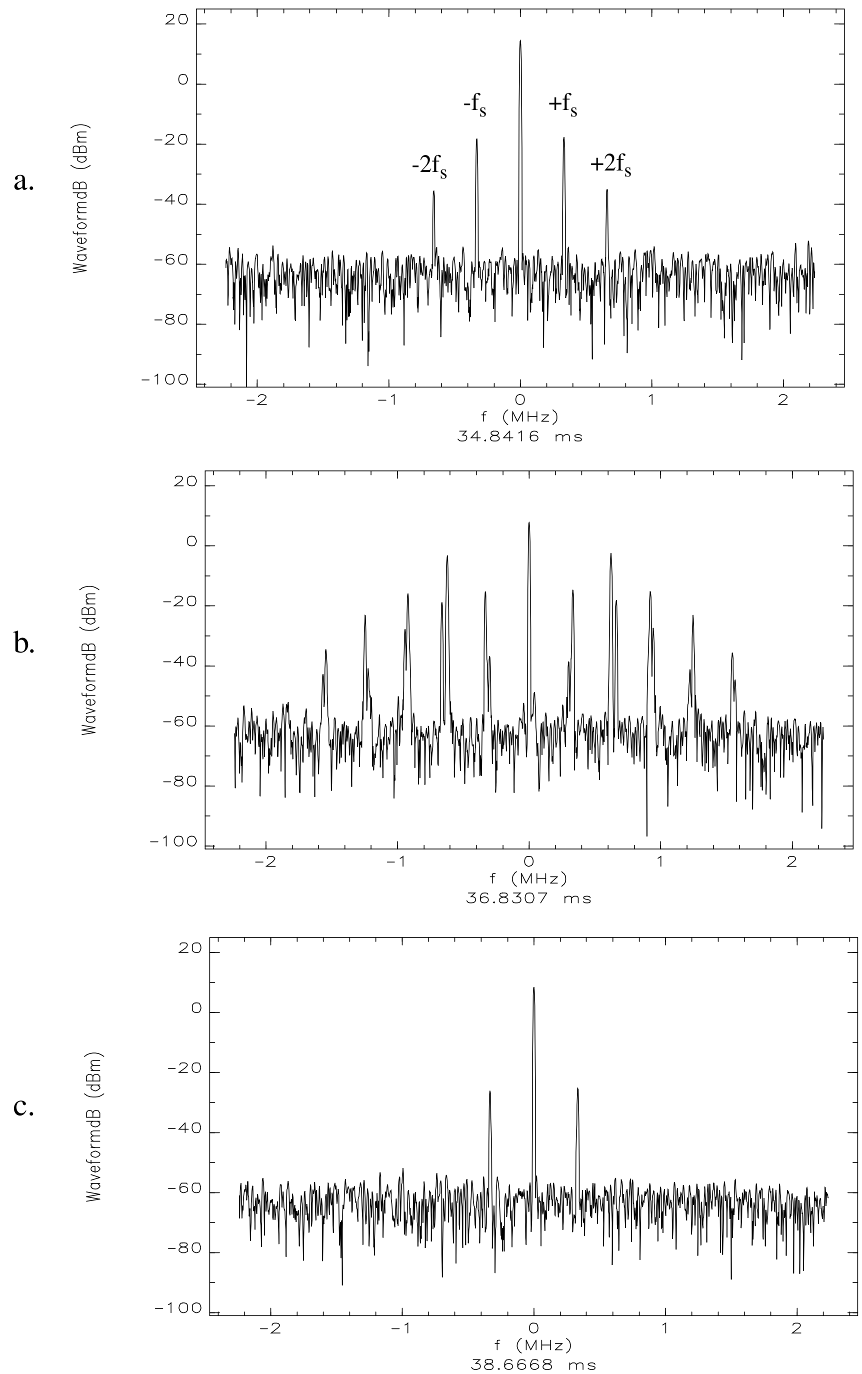

FIGURE 2. Typical synchrotron line spectra around the 3rd rf harmonic during an instability cycle. The spectra are shown at intervals of ~2 ms, where the instability (a) begins (bunch length, τ_L, min), (b) maximum amplitude (τ_L increasing), and (c) ends ($\tau_L$max). (machine condition 5)

It is clear from Fig. 2 that it is the second and higher synchrotron harmonics that are characteristic of the instability. This, as well as the cyclical bunch length variation in Fig. 1, is very similar to the so-called “sawtooth” instability observed in the SLC damping rings [8]. In SURF II, the first harmonic is present, but does not grow. The first synchrotron harmonic is referred to as the dipole mode of bunch motion, because it represents a dipole phase oscillation of the bunch centroid with respect to the stable rf phase. The second synchrotron harmonic is the quadrupole, or “breathing” mode, where the bunch length fluctuates at twice f_s. These first two modes are depicted at intervals of a quarter of a synchrotron period in Fig. 3 both in (ΔE-Δt) phase space and projected on the time axis. Higher-order motions are possible, denoted as sextupole, octupole, etc. In a system of two bunches, the individual bunch motions can be either random or coupled, in phase or out of phase in the latter case. In SURF II, the predominant synchrotron sideband signals appear at the even revolution harmonics (a residual signal at the odd harmonics can be explained by a small uneven bunch population), indicating that the coupled bunch mode is the one in which the bunch motions are in phase.

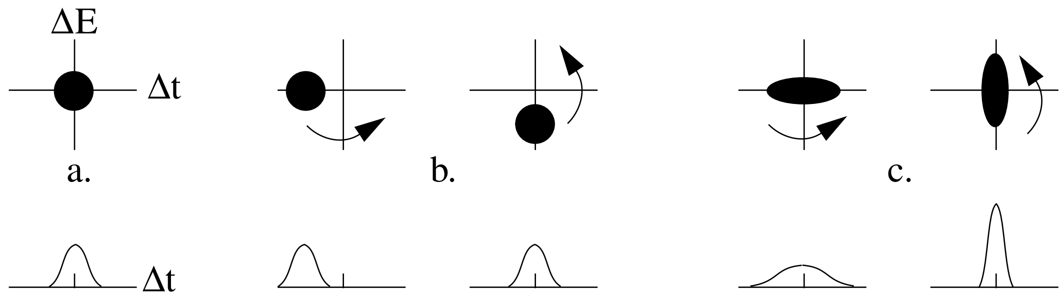

FIGURE 3. Longitudinal modes of a bunch: (a) stable, (b) dipole, and (c) quadrupole.

When the SURF beam is unstable, the quadrupole mode is observed to periodically grow in amplitude as well as shift its frequency. Figure 4 shows the growth of the quadrupole mode using the upper synchrotron sideband amplitude (lower sideband similar) plotted as a function of time for the data shown in Fig. 2. This is compared with the bunch length, which is obtained from the amplitude of the rf harmonic, assuming a Gaussian density distribution. In the figure, the bunch length is normalized to its minimum value in the dataset. One sees a “sawtooth” pattern, corresponding to the bunch length damping to its equilibrium value and then rapidly growing until finally stabilizing at a value up to 80% longer as the instability cycling occurs. The remarkable feature of this graph is that the growth of the quadrupole sideband occurs near the minimum bunch length and, hence, maximum BME signal amplitude. This can be seen in some detail in Fig. 5, which shows an exponential fit to the quadrupole mode amplitude for the first 3 ms of the instability shown in Fig. 4. The fit is reasonably good and reproduces the initial growth well, up to a value of 0.16 V, or 1.6 ns equivalent longitudinal oscillation amplitude (see Appendix A). Over about another 0.5 ms, the growth deviates from linear theory (exponential growth) until the amplitude finally saturates at a value of 0.35 V. This amplitude corresponds to an equivalent 2.2 ns longitudinal amplitude or a 0.5 MeV energy deviation. The double peak of the quadrupole mode may correspond to first one bunch becoming unstable, then the other becoming unstable at a slightly later time. This feature can be confirmed in future studies by gating the signals to measure one bunch at a time. The shift in the frequency of the quadrupole mode is shown in Fig. 6, starting almost immediately as the amplitude grows. This shift can be explained by the nonlinearities in the potential produced by the rf and any wake fields. Again, only the upper sideband is shown.

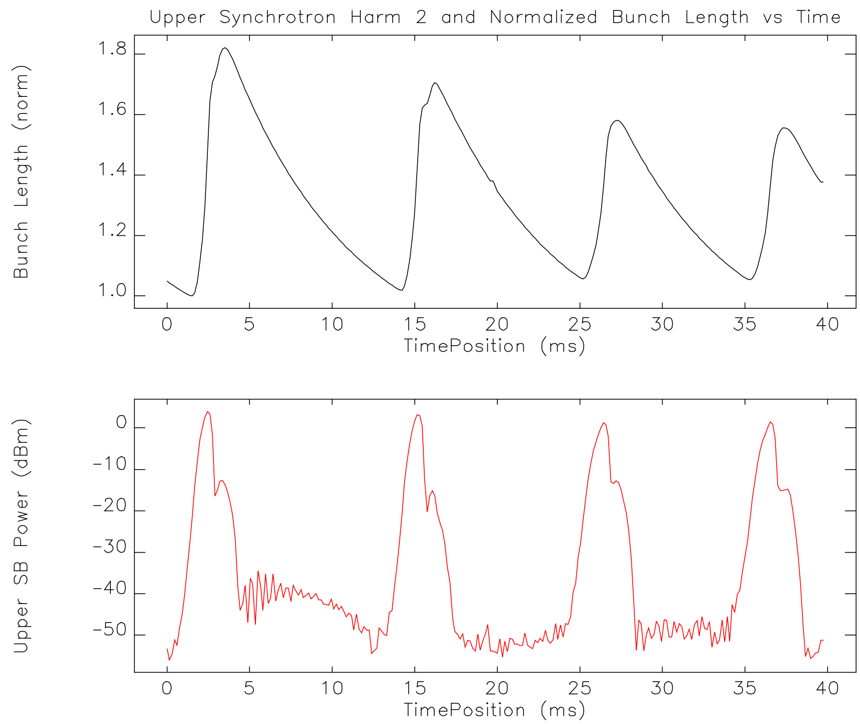

FIGURE 4. Growth of the quadrupole synchrotron harmonic with time (machine condition 5).

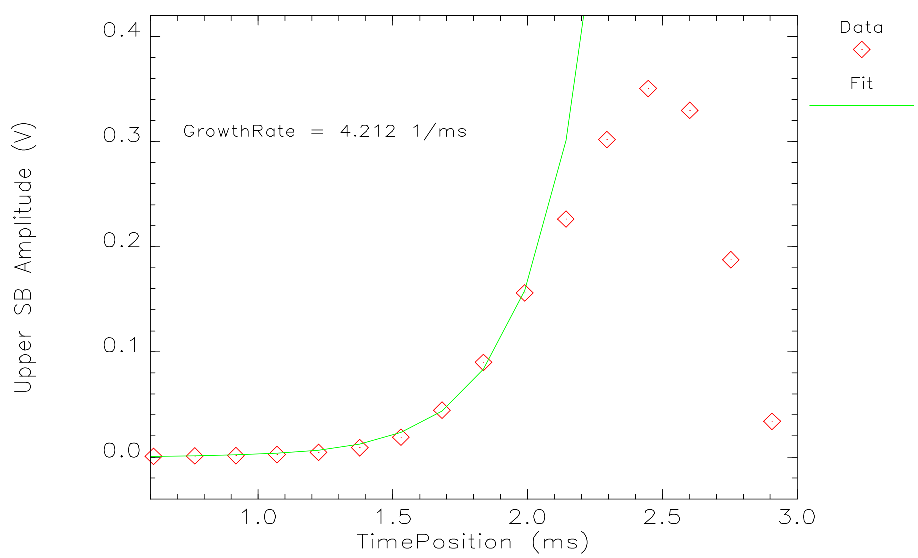

FIGURE 5. Exponential fit of quadrupole mode for the first instability cycle of Fig. 4.

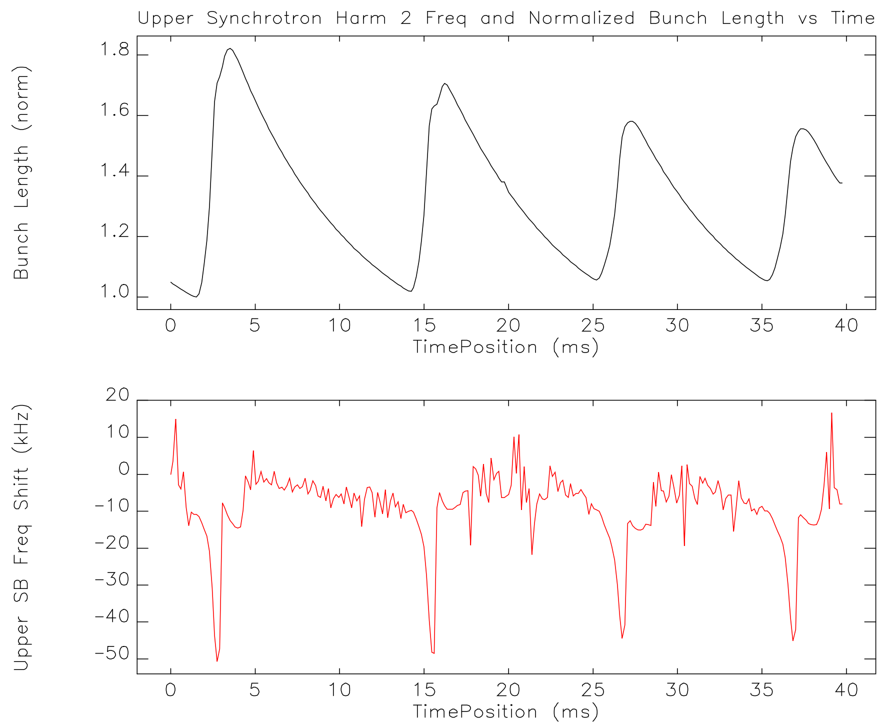

FIGURE 6. Frequency shift of the quadrupole synchrotron harmonic with time (machine condition 5).

5.0 Analysis

The growth rates for the quadrupole mode were computed and are plotted in Fig. 7. Only the even revolution harmonic spectral data were used (machine conditions 1, 2, and 5). The variation in beam intensity and bunch length (peak current) at the onset of the instability can account for the spread. This is especially true for lower beam currents (i.e., machine condition 5). The presence of two clusters of values, one around 4.5 kHz and a smaller one around 14.5 kHz, is more difficult to explain. The higher growth rates occurred for higher beam currents (machine condition 1). The Fig. 8 data (which is derived from the time domain data in Fig. 1b) shows that for high beam currents the variation in growth rates is very large. The saturation level in equivalent longitudinal amplitude of the quadrupole mode in this case ranges between 2.4 and 3.7 ns, and the bunch length grows much more rapidly in two of the three cycles. There is speculation that the instability may lead to micro-bunching, driving the local peak current to very high values, which may give rise to the higher growth rates.

It is notable that the dipole harmonic does not grow when the instability occurs. The dipole mode was not seen at all for the unstable machine conditions 1-4. When the rf phase was changed for machine condition 4, the bunch length became stable, and the dipole mode was clearly seen but with a slow fluctuation, shown in Fig. 9. The quadrupole harmonic amplitude remained constant at -15 dB compared to the rf harmonic. The dipole mode, whether induced deliberately by rf noise or resulting from the choice of rf phase, is either benign or unrelated to the bunch length fluctuation.

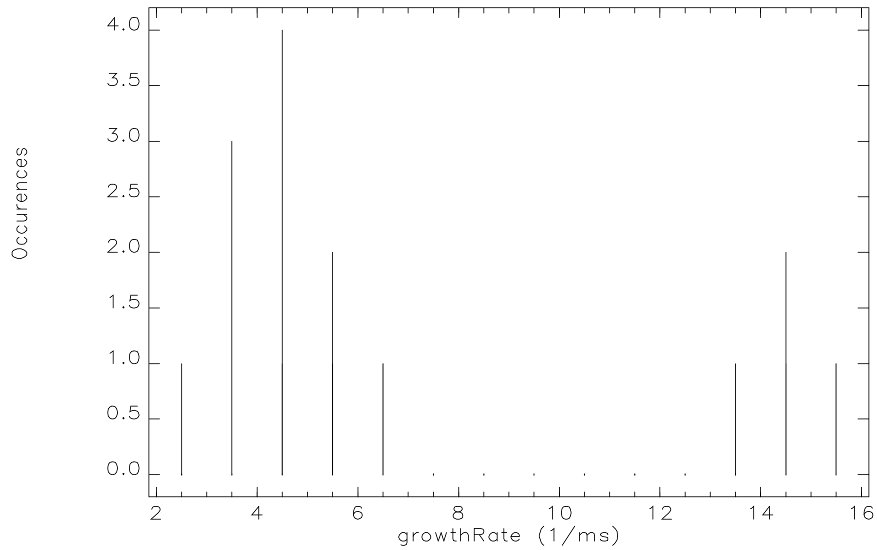

FIGURE 7. Histogram of growth rates of quadrupole mode.

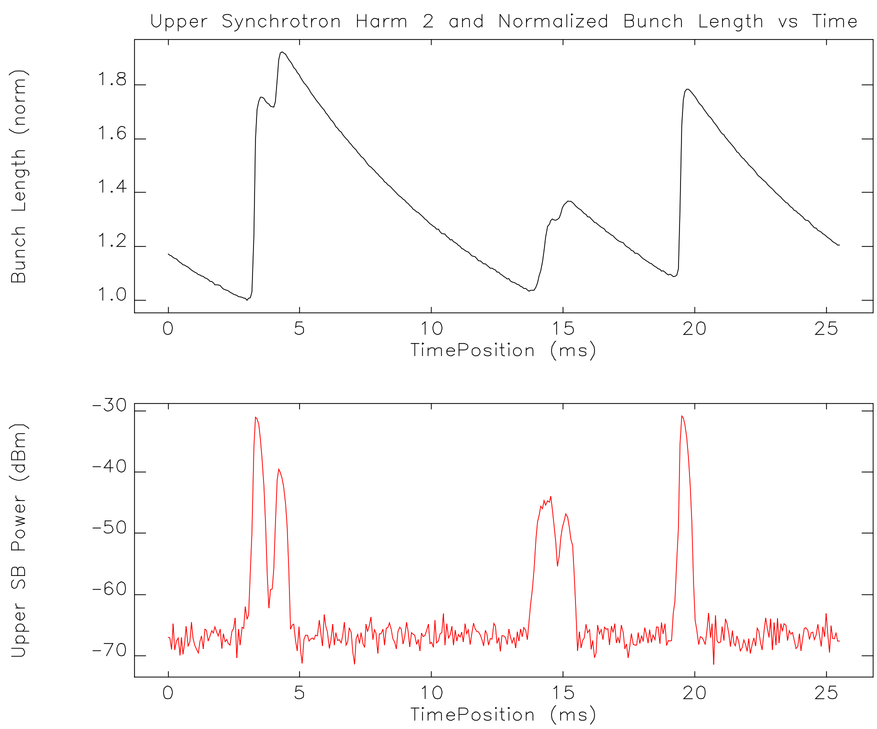

FIGURE 8. Growth of the quadrupole synchrotron harmonic with time under the same conditions as in Fig. 1b (machine condition 1).

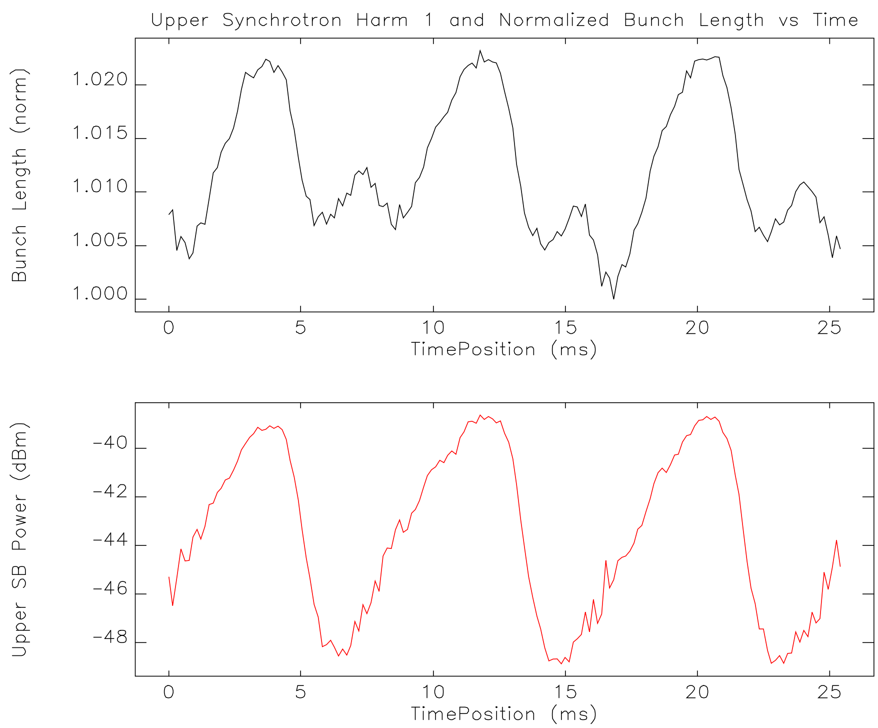

FIGURE 9. Fluctuation of the dipole synchrotron harmonic when the beam was most stable (machine condition 4).

The driving impedance giving rise to the measured growth rates can be estimated. We assume a time-dependence of $\exp(j\Gamma_m t)$. If the instability is driven by a narrowband (high Q) resonance, such as an rf cavity HOM, the growth rate, Γ_m, is given by [9][10]

$$\Gamma_m = \frac{f_s IMDF_m(\Delta\phi)}{V_{rf}\cos\phi_s Bh} R_s, \tag{2}$$

where I is the total current, M is the number of bunches, D≅1 for a high-Q resonance, B is the bunching factor (ratio of full bunch length to bunch separation), $\phi_s = \sin^{-1}(U/V_{rf})$ is the synchronous rf phase angle, and R_s is the shunt impedance for the HOM. F_m is a bunch form factor, of order unity, that is related to the Bessel functions, J_m, and depends on the bunch length. This form factor accounts for the fact that as the bunch shortens, it generates appreciable frequency components at higher frequencies, thus increasing the coupling efficiency to a HOM. The other variables are given in Table 1. Using I = 100 mA, $\cos\phi_s = 0.9990$, h = 2, and $B = 2\tau_L f_{rf} = 0.23$, and the worst-case growth rate of 15 kHz, solving Eq. 2 for the effective driving impedance, we obtain

$$R_s F_m = 0.14\ [\Omega\ \mathrm{s}]\ \Gamma_m = 2\ \mathrm{k}\Omega.$$

Rf cavity HOMs are the most likely source of coupling impedance of this magnitude in the SURF vacuum chamber. According to the standard coupled-bunch instability theory [9][10], a resonance condition must be satisfied between one or more HOM frequencies, f_{HOM}, and the harmonics (p = 1, 2, 3,...) of the rf frequency, f_{rf}; harmonics (n = 0, 1) of the revolution frequency, f_{rev}; and harmonics (m = 1, 2, 3,...) of the synchrotron frequency, f_s:

$$f_{HOM} \approx pf_{rf} \pm nf_{rev} \pm mf_s . \tag{3}$$

The quality factor, Q, of the HOM determines whether its shunt impedance is sufficient to drive the beam if the HOM frequency is close to satisfying Eq. (3).

The SURF rf cavity is a quarter-wave, folded transmission line resonant structure. The original National Bureau of Standards (NBS) SURF drawings 3-C-1035, 3-C-1038, and 3-C-1039 were used to define the cavity geometry. The code MAFIA [11] was used to calculate the fields and shunt impedances for the fundamental and HOMs. For simplicity, the cavity was assumed to be straight and the length was adjusted to obtain a fundamental frequency close to 113.8 MHz, shown in Fig. 10a. The equivalent circuit and fields are shown schematically in Figs. 10b and 10c, respectively. The shunt impedance, unloaded Q, and ratio R_s/Q_0 computed by MAFIA are given in Table 3 for the fundamental and first several longitudinal (TM) modes of the rf cavity. It should be noted that the unloaded Q does not take into account the loading by the input coupler.

a.

b.

c.

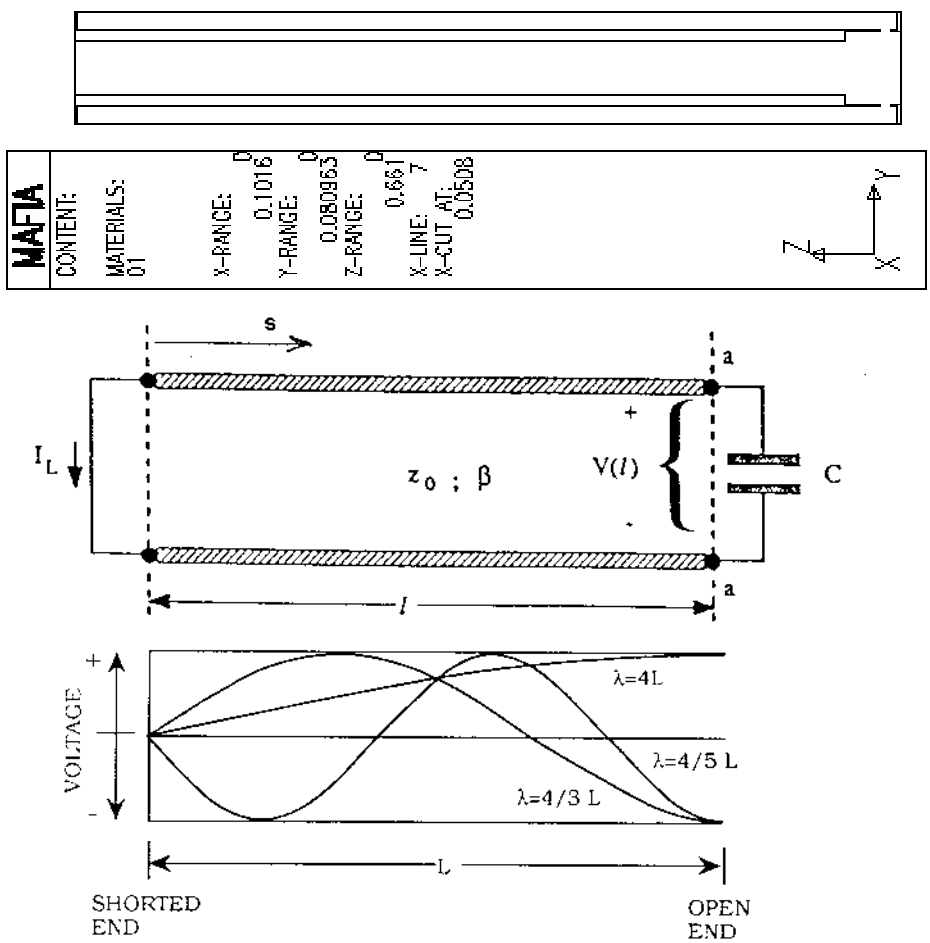

FIGURE 10. (a) Geometry (dimensions in meters), (b) equivalent transmission line [12], and (c) field patterns for a quarter-wave, coaxial cavity resonator.

The rf bench measurement results are also given in Table 3. The HOM frequencies and loaded Q's were obtained by measuring the transmission coefficients between the input coupler and a loop probe at the gap. Given that the ratio R/Q is assumed constant, the loaded shunt impedance R_L is obtained.

TABLE 3. SURF II Rf Cavity Fundamental and HOMs: Comparison of MAFIA Calculations (left) and Rf Bench Measurements (right)

freq (MHz)	R_s (kΩ)	Q_0	R_s/Q_0 (Ω)
114.06	36	2120	17.0
341.96	21	3620	5.8
569.43	17	4720	3.6
796.25	15	5560	2.7
1022.16	14	6360	2.2
1246.85	14	7000	2.0
1469.88	14	7370	1.9

freq (MHz)	Q_L	R_L (kΩ)
113.8	680	12
342.0	540	3.1
571.8	190	0.7
797.5	230	0.6
1027	143	0.3
1257	193	0.4
1462	-	-

The frequency of the 342 MHz mode is close to satisfying Eq. (3) (p=3, n=0, m=2). More importantly, its shunt impedance is high: 25% of the fundamental impedance as observed in the rf cavity bench measurements. The bunch length need not couple very strongly to this mode to give rise to an effective impedance of 2 kΩ. An additional correlation is given by the regular intervals noted earlier (about 53 deg at 7 mA) in the rf source-to-cavity phase that produced the most unstable bunch motion. This is likely correlated with one or more HOMs whose wavelength and effective transmission line length are related, giving a peak field at the gap. This effect was qualitatively verified by transmission coefficient measurements of the cavity-transmission line system. Another means of searching for the driving source is measuring the beam-driven HOM spectrum directly in the cavity assuming the cavity probe couples appreciably to the mode. These calculations and measurements show a strong correlation, but do not establish cause and effect.

6.0 Recommendations

The observations in SURF II are consistent with a short bunch producing sufficient response at one or more rf cavity HOM frequencies to generate wake fields that drive the instability. Bench measurements of the rf system, characterizing both the cavity and transmission line, were performed and a preliminary analysis supports the conclusion above. If a HOM damper can be implemented before SURF III is commissioned, further studies may be undertaken with beam to test its effectiveness. The addition of pickups and/or striplines is recommended to allow the option of implementing a feedback system at a later time, in the event that passive damping proves insufficient.

6.1 HOM damping

Passive damping is an option if a HOM is driving the beam instability, and there are a variety of possible designs. One broadband option for SURF would be to insert a band-pass filter in series in the rf transmission line and a band-reject filter in parallel with a load to ground. A schematic is shown in Fig. 11. Any reflection of the fundamental will pass as before, but any HOM-reflected power will be dissipated in the load. The HOMs closest in frequency to the fundamental should couple fairly well to the input coupler. An experiment in which the effect on the instability is observed with and without the damper should quickly verify whether rf cavity HOMs are responsible. If further damping is required, a pickup loop or flap can be placed in the rf cavity to optimize coupling to the HOM depending on the field pattern (see Fig. 10c) and minimize coupling to the fundamental, if possible. A tuned circuit is then used to reject fundamental power and pass HOM power into a load. Examples of such a narrowband HOM damper using tuned circuits and either inductive or capacitive coupling may be found in [13].

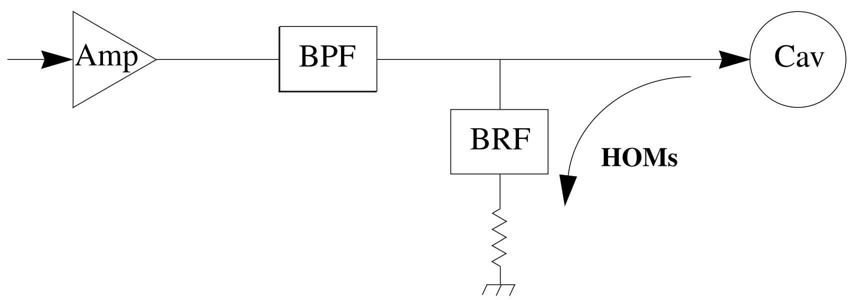

FIGURE 11. Broadband HOM damper schematic.

6.2 Longitudinal feedback system

Active damping can be pursued in the event that passive damping of HOMs does not eliminate the longitudinal coupled-bunch oscillations. The basic feedback system consists of a longitudinal kicker and pickup, bandpass filter, 90-degree phase shifter, mixer, and rf power amplifier. The pickup detects longitudinal bunch motion as a phase error at the relevant harmonic of the synchrotron frequency, and the bandpass filter acts to eliminate the large revolution harmonic signals. The pickup signal is sent to the phase shifter, which acts to produce a signal proportional to the energy error that is 90 degrees out of phase with the detected signal. The energy error signal is mixed with an appropriate multiple of the rf frequency and is passed to the rf power amplifier whose output is applied to the kicker. The rf power amplifier would need to cover a minimum bandwidth equal to half the revolution frequency (57 MHz) so as to be able to suppress any synchrotron sidebands excited by the instability. The amplifier would also need to operate at a center frequency where the kicker has a large enough response so that the kicker will be able to impress the maximum energy kick required for damping the beam.

To estimate the power and gain requirements of such a feedback system, we assume a matched stripline kicker/pickup pair with center frequency 500 MHz, bandwidth of ~200 MHz, and length 15 cm. The choice of striplines is primarily dictated by ease of fit within the existing SURF vacuum chamber while providing more than enough bandwidth to detect the relevant instability beam signals. The required maximum kicker voltage is given by [14],

$$V_k = \frac{2ET\varepsilon_{max}}{e\tau_r k_{\|}} \quad , \tag{4}$$

where E is the beam energy (up to 400 MeV SURF III upgrade), T is the revolution period, τ_r is the instability risetime, $k_{\|}$ is the longitudinal kicker constant (~1 for a stripline kicker), and ε_{max} is the maximum relative energy deviation the kicker is required to produce. The maximum power required by the kicker is given by

$$P_k = \frac{V_k^2}{2Z_o} \quad , \tag{5}$$

where Z_o is the input impedance of the stripline kicker (typically 50 Ω). Eqs. (4) and (5) show that the maximum power required to drive the kicker is determined by the machine parameters that give the fastest instability risetime and the maximum energy deviation. From Fig. 9, the fastest risetime observed is 67 µs.

An estimate of the maximum amplifier output power necessary to correct a given relative energy deviation is obtained from the machine dispersion. We assume that it would be desirable to be able to correct a horizontal position deviation of 0.5 mm (approximately 1/6th the horizontal spot size) due to energy change of the centroid of the bunch. With a machine dispersion of 2 m, the maximum energy deviation ε_{max} ~0.00025. Using these numbers in Eqs. (4) and (5) give a maximum broadband power requirement of 30 Watts (45 dBm). The minimum system gain required depends on the signal levels present at the pickup as well as various cable and component losses in the feedback system. From Fig. 2 the quadrupole synchrotron sidebands are first barely visible at approximately -60 dBm. The feedback system design must carefully take into account the noise floor level so as to amplify the small signals present at the onset of the instability.

In SURF II an amplifier was used to increase the lifetime by driving a vertical stripline pair with white noise of 14 MHz bandwidth centered on the vertical tune line. A more sophisticated feedback system could be used to damp (or anti-damp) the transverse degrees of freedom since stripline pairs can also be used to detect as well as induce transverse motion. Configuring such a feedback system to anti-damp in the vertical plane could similarly be used to increase the beam lifetime by increasing the vertical emittance via phase-space filamentation. Finally, since the ring is so small and the dispersion so large, it may be possible to damp longitudinally by kicking the beam in one of the transverse degrees of freedom. This scheme is based on the fact that the path length difference in one turn for a kicked beam is substantially longer than that for the reference orbit.

7.0 Lifetime

Operational experience at SURF shows the lifetime is much improved on driving the beam vertically with broadband noise. Lifetimes were typically short: < 1 hour for the highest currents. When broadband noise was added to the beam using vertical electrodes driven by an rf amplifier, lifetimes increased to about 2 hours at the highest stored beam currents of around 150 mA (360 mA-hr). Bunch lengthening also improves the lifetime by reducing the peak current. While the instability effectively causes the bunch length to blow up, it does so in an uncontrolled manner, and is thus a less than ideal means of improving the lifetime. Implementation of a longitudinal feedback system is likely to degrade the lifetime since the bunch length will damp to its minimum, equilibrium value. An advantage, however, is that the feedback system can be used to precisely control the bunch length. Trade-off studies can be performed to calculate how the total lifetime changes as a function of beam energy, beam current, bunch length, vacuum pressure (nominally 2 nTorr) and rf voltage, including the effects of gas scattering, Touschek effect, and quantum fluctuations.

In the absence of driven noise, using a typical measured bunch length of 1 ns (fwhm) and using the nominal machine parameters of Table 1, the lifetime for 100 mA is calculated to be 0.9 hrs. This agrees well with the observation. The lifetime is dominated by the Touschek effect when the rf voltage is ≥10 kV. If the beam is stable and damps to its natural value of 0.8 ns, the lifetime becomes 0.7 hrs. Doubling the rf voltage gives 1.2 hrs (damped τ_L = 0.5 ns). Increasing the beam energy to 400 MeV, keeping 20 kV rf voltage, gives 2.3 hrs (τ_L = 0.7 ns). Doubling the beam current to 200 mA for the latter case gives a lifetime of 1.2 hrs, and deliberately increasing the bunch length to 1 ns gives 1.7 hrs. Driving the beam vertically should improve on all these lifetimes.

8.0 Summary

Measurements of the so-called “Rakowsky” instability long observed in the storage ring at the SURF II were performed. Two features of the instability were studied under varying machine operating conditions: the sawtooth-like incoherent damping and growth of the bunch length and the time evolution of the coherent, multiple synchrotron harmonics that modulate the revolution harmonics. The latter are characteristic of longitudinal phase oscillations. Instability growth rates up to15 kHz were measured for the quadrupole mode, resulting in an estimated driving impedance of 2 kΩ. This magnitude, and the strong dependence of the instability on the phase match between the rf transmitter and the cavity, makes it highly likely that beam-excited rf cavity HOMs are driving the instability. Bench measurements of the rf cavity and transmission line qualitatively confirm this hypothesis. A simple, passive HOM damping scheme is suggested, which was used successfully at the Advanced Photon Source positron accumulator ring under the suspected HOM/coupled bunch instability scenario. Recommendations are also made to develop a feedback system to control the instability. Furthermore, the addition of beam pickups and striplines are suggested to allow implementation at a later time, if desired. Qualitatively, a correlation is observed between the longitudinal phase oscillations observed near the rf frequency and both the low frequency noise and the microwave bursts. The matter is under investigation; a detailed discussion is beyond the scope of this report.

9.0 Acknowledgments

The authors thank J. Galayda, S. Milton, M. Borland, and Y. Kang for insightful comments and suggestions, and A. Nassiri for assistance with the rf bench measurements.

The hospitality and assistance of the staff at NIST, especially C. Clark, J. Dehmer, A. Hamilton, L. Huey, T. Lucatorto, and B. Madden, is greatly appreciated.

10.0 References

[1] G. Rakowsky, "Coherent Synchrotron Relaxation Oscillation in an Electron Storage Ring," IEEE Trans. Nucl. Sci., NS-32, No. 5, 2377 (Oct. 1985).

[2] G. Rakowsky and L. Hughey, "SURF's Up at NBS: A Progress Report," IEEE Trans. Nucl. Sci., NS-26, No. 3, 3845 (Jun. 1979).

[3] F. Guzman, G. Fraser, and T. Saito, "Frequency Analysis of the Photon Beam Instability at SURF II," NIST internal report.

[4] Several texts: D. Edwards and M. Syphers, An Introduction to the Physics of High Energy Accelerators, John Wiley & Sons (1993); A. Chao, Physics of Collective Beam Instabilities in High Energy Accelerators, John Wiley & Sons (1993); H. Wiedemann, Particle Accelerator Physics, Springer-Verlag (1993); H. Wiedemann, Particle Accelerator Physics II, Springer-Verlag (1995); B. Zotter and S. Kheifets, Impedances and Wakes in High-Energy Particle Accelerators, World Scientific (1998).

[5] S. Krinsky, "Saturation of a Longitudinal Instability due to Nonlinearities of the Wake Field," Proc. 1985 Particle Accel. Conf., 2320 (May 1985).

[6] R. Madden and T. Lucatorto, private communication.

[7] R.E. Shafer, "Beam Position Monitoring," AIP Conf. Proc. 249, 601 (1992).

[8] See, for example (includes a good list of refs.): R. Baartman and M. D'Yachkov, "Simulations of Sawtooth Instability," Proc. 1995 Particle Accel. Conf., 3119 (1996).

[9] A. Hofmann, "Single-Beam Collective Phenomena -Longitudinal," CERN 77-13, Proc Theoretical Aspects of the Behavior of Beams in Accelerators and Storage Rings, Erice (Nov 1976).

[10] J. L. LaClare, "Bunched Beam Coherent Instabilities," CERN Accel School Proc., CERN 87-03, 264 (Sept. 1985).

[11] "MAFIA Users Guide," LANL Note LA-UR-90-1307 (Nov 1989).

[12] R. Baartman and S. Koscielniak, "Introduction to Rf Systems in Accelerators," course notes, U.S. Particle Accelerator School, Florida State University, (Jan 1993).

[13] D. Wildman and K. Harkay, "HOM RF Cavity Dampers for Suppressing Coupled Bunch Instabilities in the Fermilab Booster," Proc. 1993 IEEE Particle Accel. Conf., 3258 (1993).

[14] J. Galayda, "Feedback Control of Multibunch Instabilities," AIP proc 249, U.S. Particle Accelerator School, 679-680 (1989).

11.0 Appendix A: Amplitudes of Unstable Oscillations

The amplitudes of the synchrotron oscillations of a beam are extracted from the spectrum using a Fourier analysis of the time domain signal. The spectral lines for a stationary beam are given by [9]

$$S_0(\omega) = 2\pi IZ \sum_{p=-\infty}^{\infty} \delta(\omega - pM\omega_{rev}) \int_0^{\tau} J_0(pM\omega_{rev}\hat{\tau}) f_0(\hat{\tau})\hat{\tau} d\hat{\tau}, \tag{6}$$

where I is the beam current, Z is the detector impedance, p is an index, M = 2 is the total number of bunches, J_0 is a Bessel function, f_0 is the stationary particle distribution, assumed to be Gaussian, and τ is the oscillation amplitude. In a stable beam, spectral lines appear only at harmonics of the rf frequency, $\omega = pM\omega_{rev}$. Uneven bunch population gives rise to an amplitude-modulation signal at harmonics of the revolution frequency, but this will not be derived here. The integral in Eq. (6) is a form factor, F_0, giving the envelope of the amplitudes of the rf harmonics. In the case of a perturbed beam, the spectrum is that of a signal phase modulated at specific rotation harmonics, n, and is given by

$$S_m(\omega) = 2\pi IZ \sum_{p,\,m\,=\,-\infty}^{\infty} \delta(\omega - \omega_{pn} - m\omega_s - \Omega_m) i^{-m} \int_0^{\tau} J_m(\omega_{pmn}\hat{\tau}) f_m(\hat{\tau}) \hat{\tau} d\hat{\tau}, \qquad (7)$$

where m is the synchrotron mode number (see Fig. 3), $\omega_{pn} = (pM + n)\omega_{rev}$, n = 0,1 is the coupled-bunch mode index (bunch motions in phase and out-of-phase, respectively), Ω_m is defined in eqn. 2, and f_m is the perturbed particle distribution. The integral in Eq. (7) is the form factor, F_m, giving the envelope of the amplitudes of the m^{th} synchrotron sidebands.

Using $\omega_{pn} » (m\omega_s + \Omega_m)$ and n = 0, the spectra in Eqs. (6) and (7) may be compared at nearly the same frequencies. It is then possible to extract from these spectra the oscillation amplitude by taking the ratio, whereby the beam current and detector impedance drop out, leaving simply the ratio of the form factors: F_0/F_m. The difference between the amplitudes of the rf harmonic and the synchrotron sideband in the power spectra is given by the log of the square of the ratio of F_0/F_m, evaluated at $\omega = pM\omega_{rev}$, τ (in Fig. 2, for example). The form factors are evaluated numerically, and the amplitudes are found in Table 4. The equivalent energy deviation is found using the relation $\Delta t = (\alpha/2\pi f_s)\Delta E/E$, where α = 2.44 is the momentum compaction.

TABLE 4. Average, Measured Synchrotron Mode Amplitudes (ns)

machine condition	mode	at saturation	linear limit
1	quadrupole	3.7, 2.4	3.2, 2.1
4	dipole	2.3	1.25
5	quadrupole	2.20	1.6